ADVANCED OPTICAL MATERIALS
www.advopticalmat.de

Materials Views
www.MaterialsViews.com

Infrared Wavefront Control Based on Graphene Metasurfaces

*Feifei Lu, Baoan Liu, and Sheng Shen**

Metasurfaces, a new class of planar metamaterial, are attracting intensive attention due to their exceptional abilities to mold light. In this work, novel metasurfaces based on graphene nanoribbons are developed to control the wavefront of infrared light. The results show that these metasurfaces can create phase discontinuities between incident and scattered light, covering the phase range from 0 to about π while maintaining a relatively large amplitude for the scattered light. A cylindrical flat lens and anomalous refraction based on graphene nanoribbon metasurfaces are also demonstrated, paving the way to developing graphene-based tunable devices for infrared wavefront control.

1. Introduction

Graphene, a monolayer of carbon atoms arranged in a hexagonal lattice,[1] has attracted significant interest because of its superior electronic[2,3] and optical properties.[4–6] Previous studies on graphene have demonstrated that its electronic band structure are cone-shaped, and has a tunable Fermi level.[7] This unique property makes graphene a promising material for tunable optical devices,[8,9] especially in the infrared and terahertz range, such as graphene broadband modulator,[10] graphene antenna,[11] graphene photodetector,[12] and graphene plasmonic waveguide,[13] all of which have advantages over traditional devices because of their tunability and small size.

Another newly emerging research area in photonics is "metasurfaces", a technique to modify and design wavefront of electromagnetic waves for particular purposes such as anomalous reflection, optical vortex, and flat lenses.[14–16] The basic idea of metasurfaces is to create structured interfaces and introduce phase discontinuities between incident and scattered lights. Typical unit cells of a metasurface are made from noble metals to scatter incident light with selected amplitude and phase.[14] However, noble metal structures are subject to several limitations. First, while metals can couple to visible and near infrared light very strongly, the response to lower frequency electromagnetic waves are weak, limiting their applications in the infrared and terahertz range. Second, metallic unit cells are fixed structures, lacking flexibility for active control. A particularly designed metallic metasurface usually serves one purpose only. As a result, the idea of designing graphene-based metasurfaces[17,18] is attractive because of its ultra-broadband response and tunability. In this paper, we investigate optical properties of graphene nanoribbon structures and show their potential for active wavefront control. We also design a graphene nanoribbon metasurface to achieve light focusing and anomalous refraction.

F. F. Lu, B. Liu, Prof. S. Shen
Department of Mechanical Engineering
Carnegie Mellon University
5000 Forbes Avenue
Pittsburgh, PA 15213, USA
E-mail: sshen1@cmu.edu

DOI: 10.1002/adom.201400100

2. Results and Discussion

2.1. Optical Response of Graphene Nanoribbon

Graphene nanoribbons can strongly respond to infrared or terahertz electromagnetic waves due to plasmonic excitation at proper Fermi levels.[19] We employ boundary element method (BEM) to simulate the scattering of graphene nanoribbons (see Experimental Section and Supporting Information). For a proof of concept, we assume graphene ribbons to be infinitely long and freestanding. The scattering properties of a single graphene nanoribbon are presented in **Figure 1**. In our simulation, the wavelength of the light is set to be 8.6 μm and the graphene mobility is assumed to be μ = 5000 cm^2/(Vs), a typical value for exfoliated graphene samples. The light is normally incident to graphene nanoribbon, and its polarization is perpendicular to the nanoribbon direction for plasmonic excitation. Two graphene nanoribbons with different widths, 200 nm and 207 nm, are calculated for comparison.

Figure 1a shows significant phase shift between incident and scattered lights over plasmonic resonance. However, the magnetic field amplitude of the scattered light drops drastically from the resonance region. The nanoribbon width also has impact on both phase and amplitude, but a similar shift can be achieved by changing graphene Fermi level if the nanoribbon widths are comparable. This feature is of importance because in experiments, the variation of sample sizes is unavoidable, and the influence of width variation can be offset by a slight shift of Fermi level. However, the intrinsic disadvantage to use single graphene nanoribbon for metasurfaces is its incapability to provide uniform and large scattered amplitude over a wide phase range, which is crucial for wavefront control.

To overcome the drawback of a single nanoribbon, we choose to combine two parallel graphene nanoribbons (on the same plane) as a single unit cell (see the inset in **Figure 2**). More importantly, for experiments, nanoribbon or micro-ribbon structures were commonly used for exciting graphene

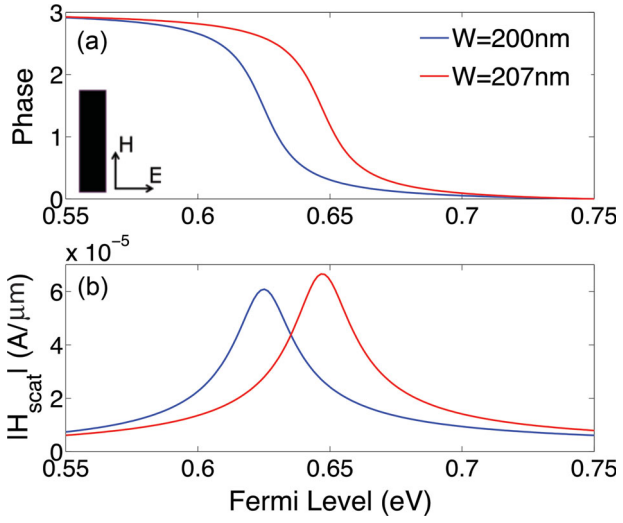

Figure 1. Optical responses of an infinitely long graphene nanoribbon. Mobility of graphene is $\mu = 5000\ cm^2/(Vs)$. The incident light has a free space wavelength of 8.6 μm and amplitude 1 V/μm. Its polarization is perpendicular to the nanoribbon (TM polarized), as shown in the inset of (a). (a) and (b) present the evolution of phase and the magnetic field amplitude of the scattered light with respect to Fermi level respectively. The result is calculated at a distance of 100 μm above the nanoribbon. The blue and red lines correspond to the results for different widths of the graphene nanoribbons, 200 nm and 207 nm, respectively.

plasmons, and their Fermi levels can be easily tuned by electrical gating.[23–25] Though multi-ribbon structures with more than two ribbons in one unit cell can also be implemented for our purpose, this simple bi-ribbon structure can be designed and simulated efficiently without loss of generality, as explained in Material and Method. Figure 2a,b show the phase shift and normalized amplitude of scattered light for a graphene unit cell comprised of two 200 nm wide nanoribbons separated by a 200 nm gap. Observation of these maps reveals that for normalized amplitude around 0.5 in Figure 2a, the corresponding regions in Figure 2b cover a wide phase range from 0 to 3, sufficient for many optical devices to control the wavefront of scattered light.

In Figure 2c, we plot several points with amplitude around half of the maximum value in Figure 2a and their corresponding phases. For the labeled points in Figure 2c, Figure 2d–i show the light intensity of graphene plasmon modes excited by transverse magnetic (TM) polarized plane wave. The energy distribution indicates very weak interaction between nanoribbons within the unit cell, no matter what Fermi levels they have.[19] As a result, the electromagnetic field scattered by this unit cell can be understood as the superposition of two single nanoribbons with a modification due to weak coupling effects between nanoribbons. Since graphene plasmonic modes are tightly localized, a gap as wide as 400–500 nm can eliminate interaction between graphene nanoribbons according to our calculation. Thus, we regard two widely separated nanoribbons as two independent units instead of one unit cell. As one example, we choose the gap size of 200 nm because the unit cell could provide relatively large scattered amplitude over a wide phase range. Based on the above results, this unit cell structure with a 200 nm gap can well serve the purpose of wavefront control, we thus use it in the following discussion and design.

2.2. Angular Dependence of Optical Response

Angular distribution of scattered light is also one important factor for designing optical devices, especially in the applications associated with large angles. We numerically calculate the scattered light at a distance R = 100 μm, and vary the angle θ to measure the angular dependence of this structure, as shown in the inset of **Figure 3**a.

When the two nanoribbons have the same Fermi level, the phase of scattered light is independent of angle, and is only a function of Fermi level. In Figure 3a, we plot the curve of phase versus Fermi level, it is similar to that of a single nanoribbon because the plasmon mode is only slightly modified by the weak coupling of the two nanoribbons. However, the magnetic field amplitude is strongly dependent on angle, as shown in Figure 3b where the amplitude profile is plotted with the Fermi level from 0.5 eV to 0.7 eV. Light is mainly scattered in the forward direction of the unit cell, and the amplitude becomes much smaller when θ increases from 0 to $\pm\pi/4$. It is noted that when Fermi level is close to plasmon resonance (about 0.65 eV), the scattered amplitude is increased dramatically, but it also becomes more sensitive to angle.

However, when $E_{f1} \neq E_{f2}$, the situation becomes more complex because both the phase and amplitude are significantly affected by angle. In Figure 3c,d, the angular dependence of the scattering amplitude is plot for different Fermi level combinations. One of the nanoribbon has a fixed Fermi level of 0.5 eV while the other has Fermi levels varying from 0.52 eV to 0.58 eV. The angular dependence is proportional to the difference between two Fermi levels. Also, the amplitude curves become slightly asymmetrical in these cases, because the difference of the two Fermi levels breaks the symmetry of the structure.

Considering the nanoribbons are simulated as infinitely thin layers, the physical structure should have little contribution to the scattering process, and we can conclude that the scattering of the nanoribbons are essentially the coupling between free space electromagnetic waves and plasmon modes supported by graphene nanoribbons. The properties and excitation efficiency of plasmonic modes, and the coupling effects between graphene nanoribbons all vary with graphene Fermi level, resulting in a Fermi level dependent angular distribution for the scattered light.

2.3. Cylindrical Flat Lens

Miniaturization is a great challenge for optical and photonic devices. Specifically, it is difficult to make traditional lens with short focal length; it is also difficult to shrink the thickness of traditional lens down to a wavelength. Several designs of flat lenses have been investigated.[20,21] Previous flat lenses are mainly based on metallic structures, and they fully take advantage of localized plasmonic modes. Considering graphene is the thinnest material, and that the mode size of graphene surface plasmons is generally one magnitude smaller than that of metal plasmons, we believe it most advantageous to utilize graphene structures for device miniaturization. Hence, we design and numerically simulate a cylindrical flat lens based

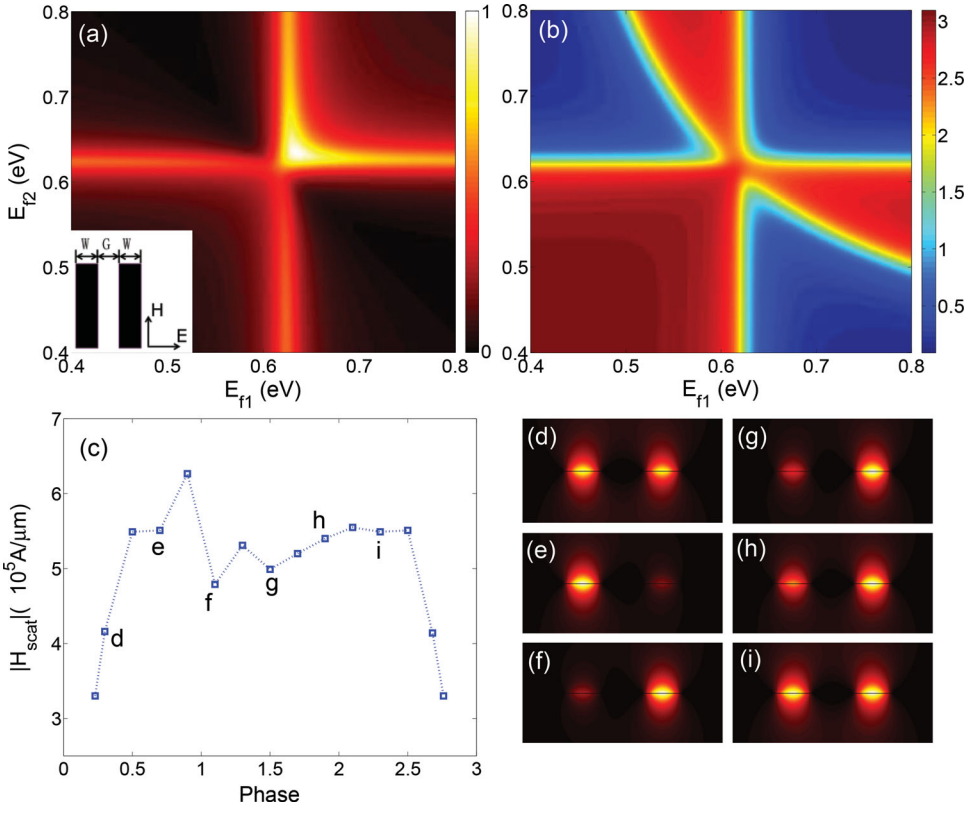

Figure 2. Optical responses of a unit cell comprised of two graphene nanoribbons. a) Normalized magnetic amplitude of scattered light, and b) phase shift with respect to the Fermi levels of two nanoribbons. The inset shows the structure of the unit cell and polarization of incident plane wave. W = 200 nm is the width of graphene nanoribbons, and G = 200 nm is the size of gap. c) A group of points picked from (a) and (b) with scattered magnetic amplitude around 5×10^{-5} A/μm. This value corresponds to half of the maximum amplitude in (a). The points in (c) cover a wide phase range from 0.2 to 2.7. d–i) Energy intensity of graphene plasmon modes excited by TM polarized plane wave. They correspond to the labeled points in (c).

on graphene nanoribbons to demonstrate the idea of wavefront control using graphene metasurfaces.

The designed cylindrical flat lens consists of 101 graphene biribbon unit cells, which are spaced 1 μm apart to avoid interaction. A TM (transverse magnetic) polarized plane wave is used to excite graphene plasmon modes of each unit cell, and the scattered electromagnetic field in the far-field region is simply the linear combination of the contributions from each unit cell because of lack of interaction. This fact significantly simplifies the design process because we have already investigated scattering properties of an independent unit cell in detail. As a result, we can select proper Fermi levels according to Figure 2 to define the phase and amplitude of light scattered by every unit cell to control the wavefront actively for multiple purposes.

In terms of the geometrical argument, light scattered by each until cell must be in phase at designed focal point, and the required phase can be predicted by

$$P(\theta, f, E_{f1}, E_{f2}) = P(\theta, R_0, E_{f1}, E_{f2}) + 2\pi \frac{f - R_0}{\lambda} \quad (1)$$

where f refers to focal length, θ is the angle from the unit cell to focal point, and $R_0 = 100$ μm is the distance where we calculate the scattered light to investigate properties of an independent unit cell. The corresponding Fermi levels can be found from Figure 2.

Figure 4a shows the results of light focusing at point (x, y) = (0,500 μm), following the above principle. However, the simulated focal length is 250 nm instead of 500 nm. The discrepancy between theory and simulation is mainly due to size effect of the lens.[20,22] When the size of a lens is not orders of magnitude larger than wavelength, Equation 1 is no longer accurate for predicting the focal length. The relative focal length shift is a function of Fresnel number $F = a^2/f\lambda$, and our simulation result is consistent with the theory proposed in previous research.[22] In Figure 4c (blue line) and 4d, two cross sections along y and x directions through the focal point are presented respectively. The full width at half maximum at the focal point is 47 μm.

Compared to traditional materials, one of the biggest advantages of graphene is its tunability. With the same device, one can conveniently tune graphene Fermi levels to achieve different focal length. In Figure 4b, we shift graphene Fermi levels and change the focal length from 250 μm to 350 μm, showing the potential of using graphene to make actively controllable devices.

2.4. Anomalous Refraction

The second example we present here to demonstrate wavefront control using graphene metasurfaces is anomalous refraction.

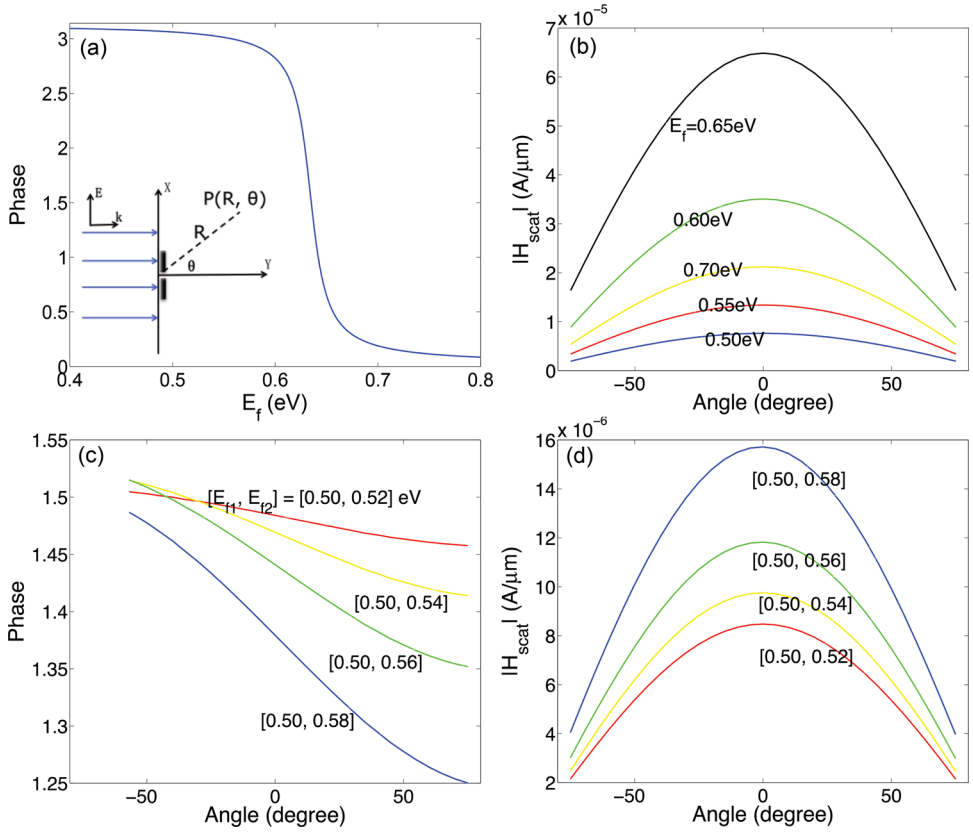

Figure 3. Angular dependence of electromagnetic field scattered by a unit cell including two graphene nanoribbons. The inset in (a) shows the scheme of the simulation, and the scattered field at point P(R, θ) is recorded, where R and θ are the distance and the angle from the unit cell, respectively. In our case, R = 100 μm. The results for $E_{f1} = E_{f2} = E_f$ are plotted in (a) and (b). When $E_{f1} = E_{f2}$, the phase of scattered light is independent of angle. The phase dependence on Fermi level is shown in (a). The amplitude dependence on angle is shown in (b). The results for $E_{f1} \neq E_{f2}$ are presented in (c) and (d), where the dependence of phase and amplitude on angle are shown respectively.

As has been proposed by Yu et al.,[14] the generalized law of refraction can be expressed by:

$$n_t \sin\theta_t - n_i \sin\theta_i = \frac{\lambda_0}{2\pi}\frac{d\varphi}{dx} \quad (2)$$

where $d\phi/dx$ refers to phase gradient along the surface. According to Equation 2, the refractive angle is tunable if we can control the phase shift at metasurface.

For normal incidence and 8.6 μm free space wavelength, a free-standing graphene metasurface could achieve a 10°

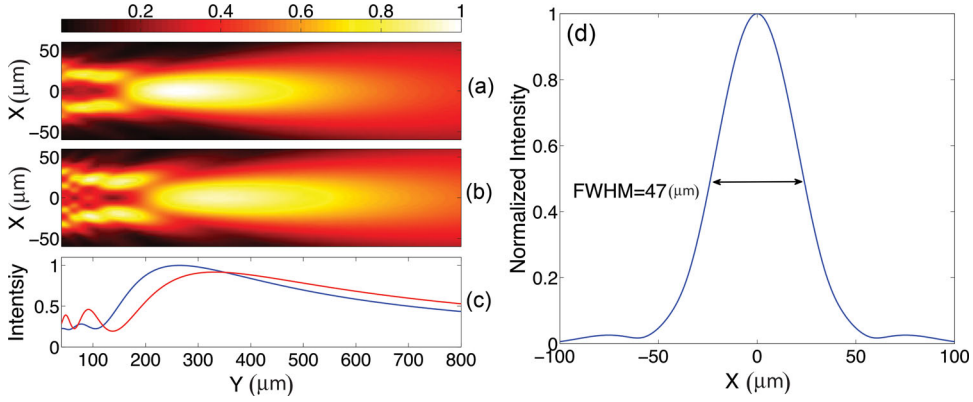

Figure 4. Simulation of a flat lens. The flat lens is composed of 101 graphene bi-nanoribbon unit cells, with 1 μm periodicity. a) Light focusing at 250 nm, and b) Light focusing at 350 nm using the same device. c) Normalized intensity along the y direction through focal point for both (a) (blue) and (b) (red). d) Intensity at the focal plane for (a).

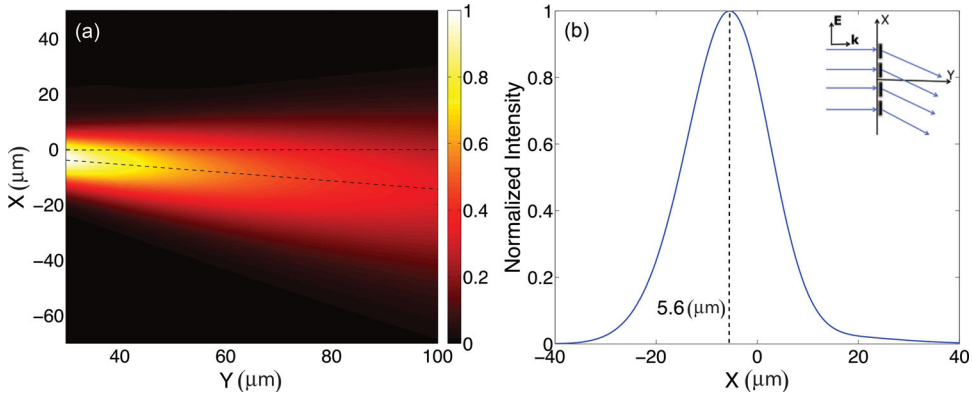

Figure 5. Anomalous refraction. a) Simulated anomalous refraction, and b) normalized intensity of light for anomalous refraction at the plane y = 40 μm. The metasurface structures are placed at x = 0 μm. The –5.6 μm deviation of the maximum intensity in (b) represents anomalous refractive angle of 8.2°.

refractive angle with 0.127 rad/μm phase gradient. In our simulation, 21 unit cells are implemented, and to avoid coupling effects, the spacing between unit cells is set to be 1 μm. The incident light is also TM polarized for plasmonic excitation. **Figure 5** shows the result of anomalous refraction. The anomalous refractive angle is about 8.2°, which is slightly smaller than our original design. Two factors are responsible for the discrepancy. First, the graphene unit cell is not diffusive, and the light scattered by each unit cell has angular distribution as discussed in this paper. Second, the size effect of the device can lead to a difference between simulated results and theoretical predictions based on geometric arguments, in which the device size is generally considered to be much larger than wavelength.

2.5. Discussion

One of the most strident criticisms of traditional metasurfaces is bandwidth limitation. This issue can be potentially solved using graphene metasurfaces for two reasons: i) graphene nanostrucures could respond to a wide range of electromagnetic waves, from near infrared to THz waves; ii) graphene Fermi level is tunable, which means for the same structure, one can change graphene properties accordingly and achieve different working wavelengths.

3. Conclusion

In this paper, we investigate the scattering properties of graphene nanoribbon and bi-ribbon graphene structures in detail. It is found that the TM polarized light scattered by a graphene bi-ribbon unit cell exhibit large amplitude over a wide phase range, making this structure a very good candidate for metasurface design and wavefront control. To numerically demonstrate the feasibility of graphene nanoribbon metasurfaces, we design and simulate a flat lens with controllable focal length and the other metasurface structure for anomalous refraction. The results in this paper demonstrate the great potential of using graphene nanoribbon based metasurfaces for active wavefront control.

4. Experimental Section

The light scattering of a single graphene nanoribbon or a graphene bi-ribbon unit cell is simulated using boundary element method (BEM). BEM is an algorithm capable of solving linear partial differential equations formulated in boundary integral form. As a result, only boundaries of a structure need to be meshed, significantly boosting calculation speed of graphene for small structures that is modeled as infinitely thin boundary layers in our case.

Since the photon energy is much smaller than $2E_f$, the optical conductivity of graphene is dominated by the intraband transition:[4]

$$\sigma(\omega) = \frac{2e^2}{\pi\hbar^2} k_B T \times \ln\left[2\cosh\left(\frac{E_f}{2k_B T}\right)\right] \frac{i}{\omega + i\tau^{-1}} \tag{3}$$

where k_B is the Boltzmann constant, $\hbar$ is the reduced Planck constant, τ is the relaxation time, and T is temperature that is set to be 300 K in out simulation.

We perform the simulations for a unit cell to obtain the information of its far field scattering properties. The data of scattered phase and magnetic amplitude are derived using a monitor, which is placed at a distance $R = 100$ μm away from the unit cell. The Fermi levels of the two nanoribbons E_{f1}, E_{f2}, as well as angle θ are scanned to calculate the phase and amplitude of the scattered light. Since the light scattered by graphene nanoribbons are physically the radiation of excited dipole modes of the nanoribbons, the scattering properties should also resemble that of dipole radiation. In far field area where $2\pi R / \lambda >> 1$, radiation amplitude of a dipole is inversely proportional to $\sqrt{R}$ in cylindrical coordinate, as a result we can derive the following relations:

$$A(\theta, R, E_{f1}, E_{f2}) = A(\theta, R_0, E_{f1}, E_{f2}) \sqrt{R_0/R} \tag{4}$$

$$P(\theta, R, E_{f1}, E_{f2}) = P(\theta, R_0, E_{f1}, E_{f2}) + 2\pi \frac{R - R_0}{\lambda} \tag{5}$$

where $R_0 = 100$ μm, $A(\theta,R_0,E_{f1},E_{f2})$ and $P(\theta,R_0,E_{f1},E_{f2})$ are recorded data in the simulations. Equation 4 follows energy conservation in cylindrical coordinate, and Equation 5 is due to additional propagation in the free space.

With these equations, we can figure out the electromagnetic field in the far-field region for an independent unit cell. Since the 1 μm periodicity in our design is large enough to avoid interaction between adjacent unit cells, the total scattered electromagnetic field in the far-field region is simply a linear combination of light scattered by each unit cell. As a result, the full simulation is no longer necessary for graphene metasurface design. Our method simplifies the design process.

Supporting Information

Supporting Information is available from the Wiley Online Library or from the author.

Acknowledgements

The authors acknowledge funding support from National Science Foundation (CBET-1253692). All the authors contributed equally to this work.

Received: March 6, 2014
Revised: May 26, 2014
Published online: June 18, 2014

[1] A. K. Geim, K. S. Novoselov, *Nat. Mater.* **2007**, *6*, 183–191.
[2] A. H. Castro Neto, F. Guinea, N. M. R. Peres, K. S. Novoselov, A. K. Geim, *Rev. Mod. Phys.* **2009**, *81*, 109–162.
[3] K. S. Novoselov, A. K. Geim, S. V. Morozov, D. Jiang, Y. Zhang, S. V. Dubonos, I. V. Grigorieva, A. A. Firsov, *Science* **2004**, *306*, 666–669.
[4] L. A. Falkovsky, S. S. Pershoguba, *Phys. Rev. B* **2007**, *76*, 153410.
[5] F. H. Koppens, D. E. Chang, F. J. Garcia de Abajo, *Nano Lett.* **2011**, *11*, 3370–3377.
[6] M. Jablan, H. Buljan, M. Soljačić, *Phys. Rev. B* **2009**, *80*, 245435.
[7] Z. Fei, A. S. Rodin, G. O. Andreev, W. Bao, A. S. McLeod, M. Wagner, L. M. Zhang, Z. Zhao, M. Thiemens,G. Dominguez, M. M. Fogler, A. H. Castro Neto, C. N. Lau, F. Keilmann, D. N. Basov, *Nature* **2012**, *487*, 82–85.
[8] A. N. Grigorenko, M. Polini, K. S. Novoselov, *Nat. Photonics* **2012**, *6*, 749–758.
[9] F. Bonaccorso, Z. Sun, T. Hasan, A. C. Ferrari, *Nat. Photonics* **2010**, *4*, 611–622.
[10] M. Liu, X. Yin, E. Ulin-Avila, B. Geng, T. Zentgraf, L. Ju, X. Zhang, *Nature* **2011**, *474*, 64–67.
[11] Z. Fang, Z. Liu, Y. Wang, P. M. Ajayan, P. Nordlander, N. J. Halas, *Nano Lett.* **2012**, *12*, 3808–3813.
[12] T. Mueller, F. Xia, P. Avouris, *Nat. Photonics* **2010**, *4*, 297–301.
[13] J. T. Kim, S. Y. Choi, *Opt. Express* **2011**, *19*, 24557–24562.
[14] N. Yu, P. Genevet, M. A. Kats, F. Aieta, J. P. Tetienne, F. Capasso, Z. Gaburro, *Science* **2011**, *334*, 333–337.
[15] P. Genevet, N. Yu, F. Aieta, J. Lin, M. A. Kats, R. Blanchard, M. O. Scully, Zeno. Gaburro, F. Capasso, *Appl. Phys. Lett.* **2012**, *100*, 013101.
[16] F. Aieta, P. Genevet, M. A. Kats, N. Yu, R. Blanchard, Z. Gaburro, F. Capasso, *Nano Lett.* **2012**, *12*, 4932–4936.
[17] A. Fallahi, J. Perruisseau-Carrier, *Phys. Rev. B* **2012**, *86*, 195408.
[18] S. H. Mousavi, I. Kholmanov, K. B. Alici, D. Purtseladze, N. Arju, K. Tatar, G. Shvets, *Nano Lett.* **2013**, *13*, 1111–1117.
[19] J. Christensen, A. Manjavacas, S. Thongrattanasiri, F. H. Koppens, F. J. Garcia de Abajo, *ACS Nano* **2011**, *6*, 431–440.
[20] L. Verslegers, P. B. Catrysse, Z. Yu, J. S. White, E. S. Barnard, M. L. Brongersma, S. Fan, *Nano Lett.* **2008**, *9*, 235–238.
[21] L. Verslegers, P. B. Catrysse, Z. Yu, S. Fan, *Appl. Phys. Lett.* **2009**, *95*, 071112–071112.
[22] Y. Gao, J. Liu, X. Zhang, Y. Wang, Y. Song, S. Liu, Y. Zhang, *Opt. Express* **2012**, *20*, 1320–1329.
[23] W. Gao, G. Shi, Z. Jin, J. Shu, Q. Zhang, R. Vajtai, Q. Xu, *Nano Lett.* **2013**, *13*, 3698–3702.
[24] L. Ju, B. Geng, J. Horng, C. Girit, M. Martin, Z. Hao, F. Wang, *Nat. Nanotechnology* **2011**, *6*, 630–634.
[25] M. Freitag, H. Y. Chiu, M. Steiner, V. Perebeinos, P. Avouris, *Nat. Nanotechnology* **2010**, *5*, 497–501.